

## Structure of $\text{Mg}_{2.56}\text{V}_{1.12}\text{W}_{0.88}\text{O}_8$ and Vibrational Raman Spectra of $\text{Mg}_{2.5}\text{VWO}_8$ and $\text{Mg}_{2.5}\text{VMoO}_8$

Jason D. Pless,<sup>§</sup> Hack-Sung Kim,<sup>§</sup> Jared P. Smit, Xiandong Wang, Peter C. Stair,\* and Kenneth R. Poeppelmeier\*

Department of Chemistry, Northwestern University, Evanston, Illinois 60208

Received October 7, 2005

$\text{Mg}_{2.56}\text{V}_{1.12}\text{W}_{0.88}\text{O}_8$  crystals were grown from a  $\text{MgO}/\text{V}_2\text{O}_5/\text{WO}_3$  melt. X-ray single-crystal diffraction studies revealed that it is orthorhombic with space group  $Pnma$ ,  $a = 5.0658(5)$  Å,  $b = 10.333(1)$  Å,  $c = 17.421(2)$  Å,  $Z = 6$ , and is isostructural with  $\text{Mg}_{2.5}\text{VMoO}_8$ . Raman spectra are reported, and the assignment of the Raman bands is made by comparing the metal–oxygen vibrations of  $\text{VO}_4/\text{WO}_4$  tetrahedra in  $\text{Mg}_{2.5}\text{VWO}_8$  with the metal–oxygen vibrations of  $\text{VO}_4/\text{MoO}_4$  tetrahedra in  $\text{Mg}_{2.5}\text{VMoO}_8$ . The stretching vibrations appearing at 1016 and 1035  $\text{cm}^{-1}$  are assigned to  $\text{Mo}=\text{O}$  and  $\text{W}=\text{O}$  double bonds, respectively, associated with the  $\text{Mg}^{2+}$  cation vacancies.

### Introduction

The selective oxidation of hydrocarbons is an important area of research for the petrochemical industry. Selective oxidation of alkanes is among the most challenging catalytic problems owing to the higher reactivity of the respective alkenes, resulting in yields that are marginal at best. The number of catalysts able to selectively break C–H bonds of low-molecular-weight alkanes is limited because of the difficulty in activating such “inert” bonds. The surfaces of mixed metal oxides with vanadium or molybdenum in isolated  $\text{MO}_4$  tetrahedra, such as  $\text{Mg}_3(\text{VO}_4)_2$  and  $\text{MgMoO}_4$ , are active in the selective oxidative dehydrogenation of alkanes.<sup>1–6</sup> Containing both vanadium and molybdenum in isolated tetrahedra,  $\text{Mg}_{2.5}\text{VMoO}_8$  exhibits conversions and selectivities for propane and butane oxidation that are similar to those of  $\text{Mg}_3(\text{VO}_4)_2$ .<sup>7,8</sup>

The structure of the mixed-metal vanadomolybdate  $\text{Mg}_{2.5+x}\text{V}_{1+2x}\text{Mo}_{1-2x}\text{O}_8$ , with vanadium and molybdenum disordered on the isolated  $(\text{V}/\text{Mo})\text{O}_4$  tetrahedra, was deter-

mined by single-crystal X-ray diffraction and powder neutron diffraction.<sup>9,10</sup> The vanadium and molybdenum cations remain in their highest oxidation states, and electrical neutrality of the crystalline framework is maintained by the partial and variable occupancy of the magnesium sites.<sup>7</sup> Similar compounds adopt this type of structure when other divalent cations are substituted for  $\text{Mg}^{2+}$ . For example, vanadomolybdates such as  $\text{Mn}_{2.47}\text{V}_{0.94}\text{Mo}_{1.06}\text{O}_8$ ,  $\text{Co}_{2.5}\text{VMoO}_8$  and  $\text{Zn}_{3.77}\text{V}_{1.54}\text{Mo}_{1.46}\text{O}_{12}$  have been synthesized.<sup>11–13</sup> Alternatively,  $\text{Mg}_{2.5}\text{VWO}_8$  is anticipated to form, owing to the similar sizes of  $\text{Mo}^{6+}$  (0.56 Å) and  $\text{W}^{6+}$  (0.55 Å) ions,<sup>14</sup> when molybdenum is replaced with tungsten.

The substitution of tungsten for molybdenum is expected to affect the acid–base, redox and catalytic properties of this phase. For example, ferric molybdate,  $\text{Fe}_2(\text{MoO}_4)_3$ , and ferric tungstate,  $\text{Fe}_2(\text{WO}_4)_3$ , are active catalysts for methanol oxidation but they are selective for different products, formaldehyde and dimethyl ether, respectively.<sup>15</sup> Similarly, the title compound provides an interesting material for comparison with the analogous molybdenum-containing catalyst.

\* To whom correspondence should be addressed. E-mail: krp@northwestern.edu (K.R.P.); pstair@northwestern.edu (P.C.S.).

<sup>§</sup> Authors with equal contributions.

- (1) Cavani, F.; Trifiro, F. *Catal. Today* **1995**, *24*, 307–313.
- (2) Mamedov, E. A.; Cortes Corberan, V. *Appl. Catal., A* **1995**, *127*, 1–40.
- (3) Bettahar, M. M.; Costentin, G.; Savary, L.; Lavalley, J. C. *Appl. Catal., A* **1996**, *145*, 1–48.
- (4) Albonetti, S.; Cavani, F.; Trifiro, F. *Catal. Rev. – Sci. Engin.* **1996**, *38*, 413–438.
- (5) Blasco, T.; Lopez Nieto, J. M. *Appl. Catal., A* **1997**, *157*, 117–142.
- (6) Kung, H. H.; Kung, M. C. *Appl. Catal., A* **1997**, *157*, 105–116.
- (7) Harding, W. D.; Kung, H. H.; Kozhevnikov, V. L.; Poeppelmeier, K. R. *J. Catal.* **1993**, *144*, 597–610.
- (8) Pless, J. D.; Ko, D.; Hammond, R. R.; Bardin, B. B.; Stair, P. C.; Poeppelmeier, K. R. *J. Catal.* **2004**, *223*, 419–431.
- (9) Wang, X. D.; Stern, C. L.; Poeppelmeier, K. R. *J. Alloy. Compd.* **1996**, *243*, 51–58.
- (10) Wang, X. D.; Pless, J. D.; Vander Griend, D. A.; Stair, P. C.; Poeppelmeier, K. R.; Hu, Z.; Jorgensen, J. D. *J. Alloy. Compd.* **2004**, *379*, 87–94.
- (11) Wang, X. D.; Heier, K. R.; Stern, C. L.; Poeppelmeier, K. R. *J. Alloy. Compd.* **1998**, *267*, 79–85.
- (12) Kurzawa, M.; Bosacka, M. *J. Therm. Anal. Calorim.* **1999**, *56*, 211–215.
- (13) Wang, X. D.; Heier, K. R.; Stern, C. L.; Poeppelmeier, K. R. *J. Alloy. Compd.* **1997**, *255*, 190–194.
- (14) Shannon, R. D.; Prewitt, C. T. *Acta Crystallogr. B* **1969**, *25*, 925–946.

The local structure and bonding of bulk and supported metal oxides (e.g., vanadates, molybdates, and tungstates) have been characterized extensively by Raman spectroscopy.<sup>16,17</sup> M=O bonded species on the surface of metal oxides are thought to play an important role in catalytic reactions.<sup>17,18</sup> However, the  $\nu_1$  stretching frequency region for MO<sub>4</sub> tetrahedra or MO<sub>6</sub> octahedra significantly overlaps with the nominal M=O stretching region of ~900–1040 cm<sup>-1</sup>,<sup>19</sup> and the vibrational frequency of the M=O stretch depends on the coordination of chemical species to the oxygen, as well as the metal.<sup>20</sup> These factors complicate the assignment of measured Raman bands. In parallel, cation vacancies in bulk crystals considerably affect the material properties.<sup>21</sup> Here the M=O bonds associated with cation vacancies in the lattice of both Mg<sub>2.5</sub>VMoO<sub>8</sub> and Mg<sub>2.5</sub>VWO<sub>8</sub> are characterized by Raman spectroscopy and single-crystal X-ray diffraction. These results provide evidence that cation vacancies in Mg<sub>2.5</sub>VMoO<sub>8</sub> and Mg<sub>2.5</sub>VWO<sub>8</sub> stabilize a M=O species that is similar to the M=O species found on oxide surfaces.

## Experimental Section

**Polycrystalline Synthesis.** MgWO<sub>4</sub> powder was prepared from MgO (99.9%, Alfa Aesar) and H<sub>2</sub>WO<sub>4</sub> (99%, Aldrich) by solid-state reaction. Stoichiometric amounts of MgO and H<sub>2</sub>WO<sub>4</sub> were ground in an agate mortar and heated at 110 °C for 5 h to drive off water from the decomposed H<sub>2</sub>WO<sub>4</sub>. The resulting powder was heated to 950 °C for 24 h in a platinum crucible. Mg<sub>3</sub>(VO<sub>4</sub>)<sub>2</sub> was synthesized from a 3:1 mole ratio of MgO and V<sub>2</sub>O<sub>5</sub> (99.6+%, Aldrich). The reactants were mixed in an agate mortar and calcined at 1000 °C for 24 h in a platinum crucible. Polycrystalline Mg<sub>2.5</sub>-VWO<sub>8</sub> was synthesized from MgO, V<sub>2</sub>O<sub>5</sub>, and H<sub>2</sub>WO<sub>4</sub> with similar procedures adopted from the preparation of MgWO<sub>4</sub>. After being mixed, the powder was calcined at 1075 °C for 36 h with one intermittent grinding. Mg<sub>2.5</sub>VMoO<sub>8</sub> was prepared from MgO, V<sub>2</sub>O<sub>5</sub>, and MoO<sub>3</sub> (99.5%, Aldrich) and calcined at 1000 °C for 24 h. Powder X-ray diffraction confirmed that all samples were single phase.

**Crystal Growth.** Mg<sub>2.56</sub>V<sub>1.12</sub>W<sub>0.88</sub>O<sub>8</sub> single crystals were grown from an initial composition of 3.732 g of MgWO<sub>4</sub> and 4.152 g of Mg<sub>3</sub>(VO<sub>4</sub>)<sub>2</sub>. A portion of the mixture was studied by differential thermal analysis (DTA). The results indicate that the sample melted incongruently at 1070 °C and became completely liquid at temperatures above 1140 °C. Accounting for the DTA results, the mixture was packed into a platinum boat and heated at 180 °C h<sup>-1</sup> to 1180 °C for 1 h, cooled to 1000 °C at 6 °C h<sup>-1</sup>, and further cooled to room temperature at 180 °C h<sup>-1</sup>. Transparent yellow needle/plate and colorless block crystals were obtained. The total weight loss was estimated to be ≤2%.

**Table 1.** Crystal Data and Details of Mg<sub>2.56</sub>V<sub>1.12</sub>W<sub>0.88</sub>O<sub>8</sub> Structure

chemical formula	Mg <sub>2.56</sub> V <sub>1.12</sub> W <sub>0.88</sub> O <sub>8</sub>
fw	409.06
cryst syst	orthorhombic
space group	<i>Pnma</i> (No. 62)
<i>a</i>	5.0658(5) Å
<i>b</i>	10.333(1) Å
<i>c</i>	17.421(2) Å
<i>V</i>	911.9(1) Å <sup>3</sup>
<i>Z</i>	6
<i>D</i> <sub>calcd</sub>	4.47 g/cm <sup>3</sup>
$\mu$ (Mo K $\alpha$ )	18.65 mm <sup>-1</sup>
radiation, wavelength	Mo K $\alpha$ , 0.71069 Å
temp	-125 °C
residuals: <i>R</i> , <i>R</i> <sub>w</sub> <sup>a</sup>	0.047, 0.051

$$^a R = \frac{\sum |F_{\text{obs}}| - |F_{\text{calcd}}|}{\sum |F_{\text{obs}}|}, R_w = \frac{[\sum w(|F_{\text{obs}}| - |F_{\text{calcd}}|)^2]}{\sum w|F_{\text{obs}}|^2}, w = 1/\sigma^2(F_{\text{obs}}).$$

**Structure Analysis.** A transparent, yellow, thin, plate crystal (0.32 × 0.20 × 0.06 mm<sup>3</sup>) was mounted on a glass fiber for study by single-crystal X-ray diffraction. All measurements were made on a Smart 1000 Bruker equipped with CCD detector and graphite-monochromated Mo K $\alpha$  radiation. Details of the structure determination and refinement are listed in Table 1. Analytical absorption corrections<sup>22</sup> were applied.

The observed systematic absences (*Ok*l, *k* + *l* = 2*n* + 1; *hk*0, *h* = 2*n* + 1) are consistent with the space groups *Pnma* and *Pn*2<sub>1</sub>*a*. The structure was solved by direct methods,<sup>23</sup> expanded using Fourier techniques<sup>24</sup> and refined satisfactorily in the centrosymmetric space group *Pnma*. Magnesium and oxygen atoms were refined anisotropically and the disordered V/W atoms were refined isotropically. Magnesium cation vacancies are localized on the Mg(2) site, and the vanadium and tungsten atoms are distributed randomly on the two tetrahedral sites M(1) and M(2). The final cycle of full-matrix least squares refinement converged with a formula Mg<sub>2.50</sub>V<sub>1.14</sub>W<sub>0.86</sub>O<sub>8</sub> and *R* = 0.046, *R*<sub>w</sub> = 0.051. To maintain charge neutrality, the final population refinement of Mg(2) was fixed at 0.420, giving a formula Mg<sub>2.56</sub>V<sub>1.12</sub>W<sub>0.88</sub>O<sub>8</sub> (*R* = 0.047 and *R*<sub>w</sub> = 0.051), which is in good agreement with the composition, Mg<sub>2.52</sub>V<sub>1.09</sub>W<sub>0.91</sub>O<sub>8</sub>, obtained by EDAX (energy dispersive analysis of X-ray). During the refinement, the constraint V(1) + W(1) = 0.5, V(2) + W(2) = 1 was used. A composition slightly rich in vanadium was expected because the melt composition resides in the vanadium-rich region for the crystal growth of Mg<sub>2.5+x</sub>V<sub>1+2x</sub>W<sub>1-2x</sub>O<sub>8</sub>. Atomic coordinates, occupancies, and thermal displacement parameters are presented in Table 2. Selected atomic distances and bond angles are given in Table 3. All calculations were performed using the TEXSAN crystallographic software package of Molecular Structure Corporation.<sup>25</sup>

**Powder X-Ray Analysis.** Powder X-ray diffraction (PXRD) patterns were recorded at room temperature on a Rigaku diffractometer (Cu K $\alpha$  radiation, Ni filter, 40 kV, 20 mA; 2 $\theta$  = 10–70°, 0.05° step size and 1 s count time) and used for crystalline phase identification. The phases were identified by comparison with the data reported in the JCPDS (Joint Committee of Powder Diffraction Standards) database.

- Machiels, C. J.; Chowdhry, U.; Sleight, A. W. *Preprints – American Chemical Society, Division of Petroleum Chemistry* **1983**, 28, 1293–1295.
- Nakamoto, K. *Infrared and Raman spectra of inorganic and coordination compounds, Part A: Theory and applications in inorganic chemistry*; John Wiley and Sons: New York, 1997.
- Stencel, J. M. *Raman spectroscopy for catalysis*; Van Nostrand Reinhold: New York, 1990.
- Wang, X. D.; Heier, K. R.; Stern, C. L.; Poeppelmeier, K. R. *Inorg. Chem.* **1998**, 37, 3252–3256.
- Mestl, G.; Srinivasan, T. K. K. *Catal. Rev. – Sci. Eng.* **1998**, 40, 451–570.
- Chan, S. S.; Wachs, I. E.; Murrell, L. L.; Wang, L.; Hall, W. K. *J. Phys. Chem.* **1984**, 88, 5831.

- Luguev, S. M.; Lugeva, N. V.; Ismailov, S. M. *High Temp.* **2004**, 42, 704–709.
- de Meulenaer, J.; Tompa, H. *Acta Crystallogr.* **1965**, 19, 1014–1018.
- Sheldrick, G. M. *SHELX86, in Crystallographic Computing 3*; Oxford University Press: New York, 1985.
- Beurskens, P. T.; Admiraal, G.; Beurskens, G.; Bosman, W. P.; de Gelder, R.; Israel, R.; Smits, J. M. M. University of Nijmegen: The Netherlands, 1994.
- TEXSAN-TEXRAY; Molecular Structure Corporation: The Woodlands, TX, 1997.

**Table 2.** Atomic Coordinates, Occupation Factors, and Temperature Parameters for  $\text{Mg}_{2.56}\text{V}_{1.12}\text{W}_{0.88}\text{O}_8$ 

atom	wyckoff position	x	y	z	Occ.	$B_{\text{eq}}^a$
W(1)	4c	0.21510(9)	0.75	0.44372(3)	0.231(2)	0.65(1) <sup>b</sup>
W(2)	8d	-0.28210(6)	0.47063(3)	0.34295(2)	0.426(3)	0.800(9) <sup>b</sup>
V(1)	4c	0.21510(9)	0.75	0.44372(3)	0.269(2)	0.65(1) <sup>b</sup>
V(2)	8d	-0.28210(6)	0.47063(3)	0.34295(2)	0.574(3)	0.800(9) <sup>b</sup>
Mg(1)	8d	-0.2503(3)	0.5758(1)	0.52663(9)	1.0	0.87(3)
Mg(2)	4c	-0.0947(9)	0.75	0.2496(2)	0.420	2.82(7)
Mg(3)	4c	0.2540(5)	0.25	0.3026(1)	0.5	1.16(5)
O(1)	8d	-0.0759(7)	0.3724(3)	0.2857(2)	1.0	1.40(7)
O(2)	8d	-0.3442(7)	0.6129(3)	0.2970(2)	1.0	1.13(6)
O(3)	8d	-0.0874(6)	0.5064(3)	0.4240(2)	1.0	1.03(6)
O(4)	8d	-0.5644(6)	0.3847(3)	0.3712(2)	1.0	1.06(6)
O(5)	4c	-0.0671(9)	0.75	0.5066(3)	0.5	1.2(1)
O(6)	8d	0.4117(7)	0.8850(3)	0.4650(2)	1.0	0.88(6)
O(7)	4c	0.1446(9)	0.75	0.3467(3)	0.5	1.4(1)

<sup>a</sup>  $B_{\text{eq}} = 8/3\pi^2(U_{11}(aa^*)^2 + U_{22}(bb^*)^2 + U_{33}(cc^*)^2 + 2U_{12}aa^*bb^* \cos \gamma + 2U_{13}aa^*cc^* \cos \beta + 2U_{23}bb^*cc^* \cos \alpha)$ . <sup>b</sup> Isotropic refinement.

**Table 3.** Selected Interatomic Distances (Å) and Bond Angles (deg) for  $\text{Mg}_{2.56}\text{V}_{1.12}\text{W}_{0.88}\text{O}_8$ 

V/W(1)–O(5)	1.80(1)	Mg(2)–O(2)	2.07(1) × 4
–O(6)	1.754(7) × 2	–O(7)	2.08(1)
–O(7)	1.73(1)	–O(7)	2.14(2)
V/W(2)–O(1)	1.765(8)	Mg(3)–O(1)	2.116(9) × 2
–O(2)	1.703(8)	–O(1)	2.170(9) × 2
–O(3)	1.762(8)	–O(4)	2.053(9) × 2
–O(4)	1.754(7)	Mg(2)–Mg(2)	2.5329(3)
Mg(1)–O(3)	2.095(8) × 2		
–O(4)	2.053(9)		
–O(5)	2.055(7)		
–O(6)	2.062(9)		
–O(6)	2.139(8)		
O(5)–V/W(1)–O(6)	108.8(3) × 2	O(1)–V/W(2)–O(3)	104.0(3)
O(5)–V/W(1)–O(7)	115.5(5)	O(1)–V/W(2)–O(4)	110.5(3)
O(6)–V/W(1)–O(6)	105.4(5)	O(2)–V/W(2)–O(3)	107.4(3)
O(6)–V/W(1)–O(7)	108.9(3) × 2	O(2)–V/W(2)–O(4)	114.7(4)
O(1)–V/W(2)–O(2)	109.9(4)	O(3)–V/W(2)–O(4)	109.7(4)

**Formation Studies.** Studies to determine the formation temperature of the  $\text{Mg}_{2.5}\text{VWO}_8$  structure were performed on a 2.5 MgO, 0.5  $\text{V}_2\text{O}_5$ , and 1.0  $\text{H}_2\text{WO}_4$  molar mixture. The sample was calcined for 24 h in air starting at 1000 °C. The sample was then cooled to room temperature and analyzed by PXRD. The temperature was increased by 25 °C every 24 h until the desired phase began to form.

**Thermal Analysis.** DTAs of the 2.5 MgO, 0.5  $\text{V}_2\text{O}_5$ , and 1.0  $\text{WO}_3$  molar mixture were made on a TA Instruments DSC 2910 differential scanning calorimeter. Measurements were made in a static air atmosphere using platinum crucibles and an alumina powder reference. The heating profile consisted of a 5 °C  $\text{min}^{-1}$  linear ramp from ambient temperature to 1150 °C. The melting point of polycrystalline  $\text{Mg}_{2.5}\text{VWO}_8$  was determined by heating the sample at 5 °C  $\text{min}^{-1}$  from room temperature to 1400 °C in a static air atmosphere. Before the measurements were made, the instrument was calibrated using indium (99.999%), zinc (99.999%), silver (99.99%), and gold (99.99%) standards.

**Elemental Analysis.** The needle/plate and block crystals were analyzed by EDAX on a Hitachi, Pioneer S-4500 SEM. The Mg/V/W average atomic ratio of the needle/plate crystals was determined to be 2.52:1.09:0.91. The average atomic ratio of Mg/V/W for the block crystals was determined to be 3.01:1.98:0.00, indicating  $\text{Mg}_3(\text{VO}_4)_2$ .

**Raman Spectroscopy.** Unpolarized Raman (100–1200  $\text{cm}^{-1}$ ) spectra of polycrystalline  $\text{Mg}_{2.5}\text{VWO}_8$  and  $\text{Mg}_{2.5}\text{VMoO}_8$  were collected on a Bio-Rad FT-Raman spectrophotometer with 0.5  $\text{cm}^{-1}$  resolution (150 scans).

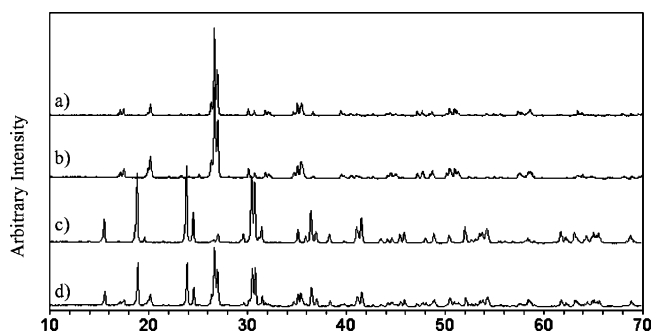


**Figure 1.** Powder diffraction patterns for  $\text{Mg}_{2.5}\text{VMoO}_8$  and  $\text{Mg}_{2.5}\text{VWO}_8$ . The samples were prepared from stoichiometric amounts of MgO,  $\text{V}_2\text{O}_5$ , and  $\text{WO}_3$  or  $\text{MoO}_3$ . The samples were calcined for 24 h at various temperatures: (a)  $\text{Mg}_{2.5}\text{VMoO}_8$ , 1000 °C; (b)  $\text{Mg}_{2.5}\text{VWO}_8$ , 1075 °C; (c) 1:2 molar mixture of  $\text{Mg}_3(\text{VO}_4)_2$  and  $\text{MgWO}_4$ , 1000 °C; and (d) mixture of  $\text{Mg}_{2.5}\text{VWO}_8$ ,  $\text{Mg}_3(\text{VO}_4)_2$  and  $\text{MgWO}_4$ , 1025 °C. The diffraction patterns were taken at ambient temperature in air.

## Results and Discussion

**Synthesis of  $\text{Mg}_{2.5}\text{VWO}_8$ .** The formation of  $\text{Mg}_{2.5}\text{VWO}_8$  was examined using PXRD; the XRD pattern of  $\text{Mg}_{2.5}\text{VWO}_8$  is similar to that of  $\text{Mg}_{2.5}\text{VMoO}_8$ <sup>26</sup> (Figure 1). Diffraction patterns of the 2.5 MgO, 0.5  $\text{V}_2\text{O}_5$ , and 1.0  $\text{H}_2\text{WO}_4$  molar mixture calcined for 24 h at various temperatures reveal that a mixture of  $\text{Mg}_3(\text{VO}_4)_2$  and  $\text{MgWO}_4$  is present in samples calcined below 1025 °C.  $\text{Mg}_{2.5}\text{VWO}_8$  was detected initially at 1025 °C. Single-phase samples can be obtained after heating at about 1075 °C for 24 h.

Investigation of  $\text{Mg}_{2.5}\text{VWO}_8$  by DTA indicates that polycrystalline  $\text{Mg}_{2.5}\text{VWO}_8$  melts at about 1219 °C. The PXRD results suggest that the  $\text{Mg}_{2.5}\text{VWO}_8$  structure begins to form at an appreciable rate at 1025 °C, or approximately 200 °C below its melting point. Similar behavior was reported for the analogous phases  $\text{Mg}_{2.5}\text{VMoO}_8$  and  $\text{Zn}_{2.5}\text{VMoO}_8$ .<sup>10,27,28</sup>

Since various examples are known with the  $\text{Mg}_{2.5}\text{VMoO}_8$  structure type, substitution of various divalent cations for

(26) Zubkov, V. G.; Leonidov, I. A.; Poeppelmeier, K. R.; Kozhevnikov, V. L. *J. Solid State Chem.* **1994**, *111*, 197–201.

(27) Kurzawa, M.; Bosacka, M. *J. Therm. Anal. Calorim.* **2001**, *64*, 1081–1085.

(28) Tabero, P.; Bosacka, M.; Kurzawa, M. *J. Therm. Anal. Calorim.* **2001**, *65*, 865–869.

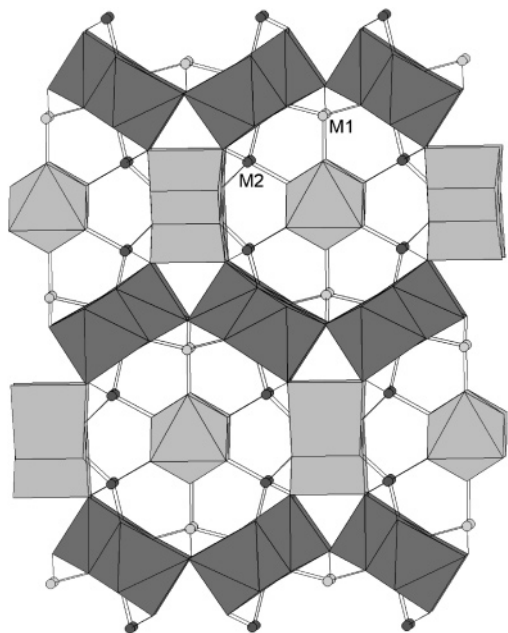


**Figure 2.** General structure of Mg<sub>2.5</sub>VWO<sub>8</sub>. The small circles marked M1 and M2 are the V/W sites. MgO<sub>6</sub> polyhedra are shown as dark gray octahedra and light gray trigonal prisms.

Mg<sup>2+</sup> in Mg<sub>2.5</sub>VWO<sub>8</sub> was anticipated. Attempts to form the Mn<sup>2+</sup>, Zn<sup>2+</sup>, and Co<sup>2+</sup> analogues by solid-state synthesis techniques resulted in mixtures of M<sub>3</sub>(VO<sub>4</sub>)<sub>2</sub> and MWO<sub>4</sub> (M = Mn, Co, Zn). These results follow a previously observed trend with molybdates and tungstates. For example, many divalent cations are known to form Li<sub>2</sub>M<sub>2</sub>(MoO<sub>4</sub>)<sub>3</sub> (M = Mg, Mn, Fe, Co, Ni, Cu, Zn),<sup>29–32</sup> whereas, in contrast, Li<sub>2</sub>Mg<sub>2</sub>(WO<sub>4</sub>)<sub>3</sub><sup>33</sup> is the only stable tungstate homeotype.

**Structural Description of Mg<sub>2.56</sub>V<sub>1.12</sub>W<sub>0.88</sub>O<sub>8</sub>.** Mg<sub>2.56</sub>V<sub>1.12</sub>W<sub>0.88</sub>O<sub>8</sub> is isostructural with Mg<sub>2.54</sub>V<sub>1.08</sub>Mo<sub>0.92</sub>O<sub>8</sub> and Mn<sub>2.47</sub>V<sub>0.94</sub>Mo<sub>1.06</sub>O<sub>8</sub> and is closely related to Zn<sub>3.77</sub>V<sub>1.54</sub>Mo<sub>1.46</sub>O<sub>12</sub> (Figure 2).<sup>9,11,13</sup> The structure is composed of two crystallographically distinct MgO<sub>6</sub> octahedra, a MgO<sub>6</sub> trigonal prism, and two crystallographically inequivalent (V/W)O<sub>4</sub> tetrahedra. The vanadium and tungsten are disordered on the tetrahedral sites. These tetrahedra are linked to the various MgO<sub>6</sub> polyhedra by corner-sharing and form a three-dimensional framework. The complete structure can be described as isolated (V/W)O<sub>4</sub> tetrahedra connected to the inner wall of the hexagonal tunnels formed by the Mg(1)O<sub>6</sub> octahedra and Mg(3)O<sub>6</sub> trigonal prisms with infinite chains of face sharing Mg(2)O<sub>6</sub> octahedra passing through the center of these tunnels (Figure 2).

Compared to Mg<sub>2.54</sub>V<sub>1.08</sub>Mo<sub>0.92</sub>O<sub>8</sub>, the *a* axis increased only 0.007 Å and the *b* and *c* axes are increased about 0.03 and 0.02 Å, respectively.<sup>9</sup> The (V/W)–O bond lengths (1.70–1.80 Å, Table 3) of the disordered (V/W)O<sub>4</sub> tetrahedra are

(29) Efremov, V. A.; Trunov, V. K. *Russ. J. Inorg. Chem.* **1972**, *17*, 1055–1058.

(30) Ozima, M.; Sato, S.; Zoltai, T. *Acta Crystallogr. B* **1977**, *33*, 2175–2181.

(31) Wanklyn, B. M.; Wondre, F. R.; Davison, W. *J. Mater. Sci.* **1976**, *11*, 1607–1614.

(32) Penkova, V. G.; Klevtsov, P. V. *Russ. J. Inorg. Chem.* **1977**, *22*, 930–931.

(33) Fu, Z.; Li, W. *Powder Diffr.* **1994**, *9*, 158–160.

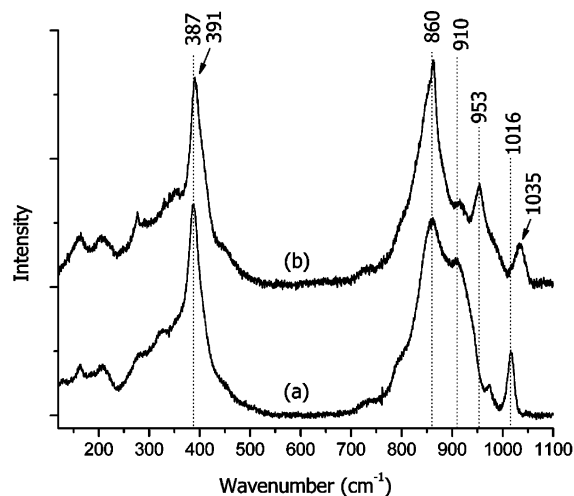


**Figure 3.** Raman spectra of isostructural (a) Mg<sub>2.5</sub>VMO<sub>8</sub> and (b) Mg<sub>2.5</sub>VWO<sub>8</sub>.

similar to the (V/Mo)–O bond lengths of the disordered (V/Mo)O<sub>4</sub> tetrahedra in Mg<sub>2.54</sub>V<sub>1.08</sub>Mo<sub>0.92</sub>O<sub>8</sub> (1.71–1.77 Å).<sup>9</sup> Bond valence calculations<sup>34</sup> for the (V/W) positions (M1 and M2) result in M1 = +5.3 and M2 = +5.5. These bond valences are consistent with a model where the V<sup>5+</sup> and W<sup>6+</sup> are statistically disordered on the two tetrahedral sites. The Mg–O bond lengths (2.05–2.17 Å) for the three MgO<sub>6</sub> polyhedra compare well with those reported for the molybdenum analogue (2.04–2.18 Å).<sup>9</sup> Magnesium cation vacancies are located within the face-shared octahedra, similar to Mg<sub>2.54</sub>V<sub>1.08</sub>Mo<sub>0.92</sub>O<sub>8</sub>. The average short Mg(2)–Mg(2) distance of 2.533 Å is the likely reason for the localization of the cation vacancies on the Mg(2) sites. The relatively large thermal displacements (see Table 2) along the *a* axis for Mg(2) are attributed to the displacement of Mg<sup>2+</sup> ions, arising from coulombic repulsions, toward adjacent vacant octahedral sites.

**Raman Studies.** Figure 3 shows the Raman spectra of Mg<sub>2.5</sub>VWO<sub>8</sub> and Mg<sub>2.5</sub>VMO<sub>8</sub>. Vibrational analysis can be performed by site group analysis, factor group analysis, and the correlation method, with the three methods giving the same result.<sup>16</sup> The *Pnma* space group of the orthorhombic crystals has the *D*<sub>2h</sub> factor group. The internal vibrational modes of the *D*<sub>2h</sub> factor group consist of A<sub>g</sub>, B<sub>g</sub>, A<sub>u</sub>, and B<sub>u</sub>.<sup>35</sup> The in-phase vibrations (A<sub>g</sub> and B<sub>g</sub>) are Raman active and the out-of phase modes (A<sub>u</sub> and B<sub>u</sub>) are IR active, since the mutual exclusion principle holds within the crystal.

A simplified structural model of Mg<sub>2.5</sub>VWO<sub>8</sub> and Mg<sub>2.5</sub>VMO<sub>8</sub> which is composed of Mg<sup>2+</sup> and tetrahedral (V/Mo/W)O<sub>4</sub><sup>2-</sup> sublattices occupying the *D*<sub>2h</sub> symmetry sites can be considered. The internal vibrational modes of the free tetrahedral molecule/ion with *T*<sub>d</sub> symmetry are classified as ν<sub>1</sub> (the symmetric stretching mode of A<sub>1</sub> symmetry), ν<sub>2</sub> (the bending mode of E symmetry), ν<sub>3</sub> (the antisymmetric stretching mode of T<sub>2</sub> symmetry), and ν<sub>4</sub> (the bending mode of T<sub>2</sub> symmetry), all four vibrations are Raman active. The ν<sub>1</sub> (A<sub>1</sub>), ν<sub>2</sub> (E), ν<sub>3</sub> (T<sub>2</sub>), and ν<sub>4</sub> (T<sub>2</sub>) modes of the orthorhombic

(34) Brown, I. D.; Altermatt, D. *Acta Crystallogr. B* **1985**, *41*, 244–247.

(35) Maczka, M. *J. Raman Spectrosc.* **1999**, *22*, 971–980.

phase with the  $D_{2h}$  symmetry split into  $A_g$ ,  $2A_g$ ,  $B_{1g} + B_{2g} + B_{3g}$ , and  $B_{1g} + B_{2g} + B_{3g}$ , respectively.<sup>16</sup>

The symmetric  $\nu_1(A_1)$  mode for the tetrahedral ions is the most intense among the four Raman active modes. The relative Raman intensities of  $\nu_1(A_1)$  mode for the various tetrahedra were measured using the  $\nu_1(A_1)$  mode of the perchlorate ion as an internal standard (its Raman intensity is normalized to 1.00) and decrease as follows.  $\text{VO}_4^{3-}$  (1.74) >  $\text{MoO}_4^{2-}$  (1.38) >  $\text{WO}_4^{2-}$  (1.11).<sup>36</sup> In addition, the Raman band positions of  $\nu_1(A_1)$  mode in aqueous solution increase as follows.  $\text{VO}_4^{3-}$  (826  $\text{cm}^{-1}$ ) <  $\text{MoO}_4^{2-}$  (897  $\text{cm}^{-1}$ ) <  $\text{WO}_4^{2-}$  (931  $\text{cm}^{-1}$ ).<sup>37</sup> The  $\nu_1(A_1)$  band positions of  $\text{VO}_4^{3-}$  tetrahedra for crystalline  $\text{MVO}_4$  (M is a trivalent ion) were frequently observed at higher frequencies than in the aqueous solution. For example, the  $\nu_1$  band position of the  $\text{VO}_4^{3-}$  tetrahedra for  $\text{CeVO}_4$  powder was observed at 859  $\text{cm}^{-1}$ ,<sup>38</sup> which is almost identical to those of  $\text{Mg}_{2.5}\text{VMoO}_8$  and  $\text{Mg}_{2.5}\text{VWO}_8$ . Thus, the band at 860  $\text{cm}^{-1}$  is assigned to the  $\nu_1$  mode ( $A_1$  in  $T_d$  point group,  $A_g$  in the  $D_{2h}$  space group) of the  $\text{VO}_4$  tetrahedra because it is the strongest in relative intensity, lowest in position in the 750–1050  $\text{cm}^{-1}$  region, and appeared in the two Raman spectra for  $\text{Mg}_{2.5}(\text{VO}_4)$ - $(\text{MoO}_4)$  and  $\text{Mg}_{2.5}(\text{VO}_4)(\text{WO}_4)$ . Further evidence for the assignment of the band is provided by separate Raman measurements for vanadia-free, but isostructural,  $\text{Li}_2\text{Mg}_2(\text{MoO}_4)_3$ .<sup>39</sup>

The second strongest and higher-frequency bands centered at 910 and 953  $\text{cm}^{-1}$ , in the 750–1050  $\text{cm}^{-1}$  region of the Raman spectra for  $\text{Mg}_{2.5}\text{VMoO}_8$  and  $\text{Mg}_{2.5}\text{VWO}_8$ , are assigned to the  $\nu_1$  mode of the distorted  $\text{MoO}_4^{2-}$  and  $\text{WO}_4^{2-}$  tetrahedra, respectively. The bands are in general agreement, in terms of positions and relative intensities, with the strong bands observed at 897 and 934  $\text{cm}^{-1}$  for tetrahedral  $\text{MoO}_4^{2-}$  and  $\text{WO}_4^{2-}$  in the respective  $\text{KLa}_{0.9}\text{Tm}_{0.1}(\text{MoO}_4)_2$  and  $\text{KLa}_{0.9}\text{Tm}_{0.1}(\text{WO}_4)_2$  compounds.<sup>40</sup> The assignment of the band at 910  $\text{cm}^{-1}$  as  $\nu_1(A_1)$  of  $\text{MoO}_4^{2-}$  is further supported by Raman measurements obtained for the  $\text{Li}_2\text{Mg}_2(\text{MoO}_4)_3$ - $\text{Mg}_{2.5}\text{VMoO}_8$  solid solution in a companion paper.<sup>39</sup>

The  $\nu_2$  band positions of the aqueous  $\text{VO}_4^{3-}$ ,  $\text{MoO}_4^{2-}$ , and  $\text{WO}_4^{2-}$  tetrahedra are similar, i.e., 336, 317, and 325  $\text{cm}^{-1}$ , respectively, and are estimated to overlap with the  $\nu_4$  band positions.<sup>16</sup> The  $\nu_2$  band positions of the  $\text{VO}_4^{3-}$  tetrahedra for the single crystalline  $\text{PrVO}_4$ ,  $\text{NdVO}_4$ , and  $\text{ErVO}_4$  were observed to be almost the same at 381, 381, and 385  $\text{cm}^{-1}$ , respectively.<sup>41</sup> Thus, the strong bands appearing at 387 and 391  $\text{cm}^{-1}$ , shown in Figure 3, should be attributed to the bending ( $\nu_2(E)$  and/or  $\nu_4(T_2)$ ) mode of the  $\text{VO}_4$ ,  $\text{MoO}_4$ , and  $\text{WO}_4$  tetrahedra present in  $\text{Mg}_{2.5}\text{VMoO}_8$  and  $\text{Mg}_{2.5}\text{VWO}_8$ . Since the Raman intensity of a band at 387  $\text{cm}^{-1}$  was

observed to be proportional to the concentration of vanadia in solid solutions,<sup>39</sup> the band at 387  $\text{cm}^{-1}$  was assigned to bending vibrations of  $\text{VO}_4$  tetrahedra in  $\text{Mg}_{2.5}\text{VMoO}_8$ . Thus, the strong band at 391  $\text{cm}^{-1}$ , which is close to 387  $\text{cm}^{-1}$ , should be attributed to the bending mode of the  $\text{VO}_4$  tetrahedra present in  $\text{Mg}_{2.5}\text{VWO}_8$ . Accordingly, shoulder bands appearing at  $\sim 330$ – $370$   $\text{cm}^{-1}$  in the Raman spectra of  $\text{Mg}_{2.5}\text{VMoO}_8$  and  $\text{Mg}_{2.5}\text{VWO}_8$  can be assigned to the bending mode of the  $\text{MoO}_4$  and  $\text{WO}_4$  tetrahedra in  $\text{Mg}_{2.5}\text{VMoO}_8$  and  $\text{Mg}_{2.5}\text{VWO}_8$ . A separate Raman study indicates that the bending mode of the  $\text{MoO}_4$  tetrahedra in  $\text{Mg}_{2.5}\text{VMoO}_8$  appears at 326 and 370  $\text{cm}^{-1}$ .<sup>39</sup>

The antisymmetric stretching  $\nu_3$  vibration of the aqueous  $\text{VO}_4^{3-}$ ,  $\text{MoO}_4^{2-}$ , and  $\text{WO}_4^{2-}$  tetrahedra was observed by Raman spectroscopy at 804, 837, and 838  $\text{cm}^{-1}$ , lower in position than their symmetric stretching  $\nu_1$  vibrations, 826, 897, and 931  $\text{cm}^{-1}$ , respectively.<sup>37</sup> Therefore, the shoulder band appearing about 795  $\text{cm}^{-1}$  is likely to be the  $\nu_3$  mode of the  $\text{VO}_4$  tetrahedra present both in  $\text{Mg}_{2.5}\text{VMoO}_8$  and  $\text{Mg}_{2.5}\text{VWO}_8$ .

Additional structural information concerning the distortion of the tetrahedron can be obtained from the Raman spectra. Hardcastle and Wachs reported that an increase in the Raman frequency associated with the highest  $\nu_1$  symmetric stretching mode of tetrahedrally or octahedrally coordinated molybdate and tungstate species correlates to a decrease in the Mo–O<sup>42</sup> or W–O bond length.<sup>43</sup> The Raman frequency follows the empirical correlation:  $\nu$  (in  $\text{cm}^{-1}$ ) = 32 895  $\exp(-2.073R_{\text{Mo}})$  or 25 823  $\exp(-1.902R_{\text{W}})$ , where  $R_{\text{Mo}}$  and  $R_{\text{W}}$  are the Mo–O and W–O bond distances, respectively, in Å.<sup>43</sup> Additionally, the degree of angular distortion of the polyhedral structure is an important variable for the Mo–O or W–O stretching Raman frequency.<sup>43</sup> For example,  $\beta$ - $\text{Bi}_2\text{Mo}_2\text{O}_9$  with slightly distorted  $\text{MoO}_4$  tetrahedral angles and  $\text{FeMoO}_4\text{Cl}$  with highly distorted  $\text{MoO}_4$  tetrahedral angles have exactly the same Mo–O bond lengths of 1.756 Å, but they show very different highest Raman frequencies at 887 and 975  $\text{cm}^{-1}$ , respectively, owing to the very different degree of tetrahedral angular distortion.  $\text{PbWO}_4$  with almost perfect  $\text{WO}_4$  tetrahedral coordination and  $\text{Li}_2\text{WO}_4$  with highly distorted  $\text{WO}_4$  tetrahedral coordination have exactly the same W–O bond lengths of 1.77 Å, but they show very different highest Raman frequencies at 902 and 963  $\text{cm}^{-1}$ , respectively.<sup>43</sup> Therefore, the Mo–O or W–O stretching vibrations blue-shift with either a higher degree of polyhedral angular distortion or with shorter Mo–O or W–O bond lengths, and vice versa. The W–O bond length (1.75 Å in average,  $\nu_1$  at 953  $\text{cm}^{-1}$ ) of  $\text{WO}_4$  tetrahedra with distorted angles in  $\text{Mg}_{2.5}\text{VWO}_8$  is very similar to the W–O bond length of  $\text{WO}_4$  tetrahedra with distorted angles in  $\text{K}_2\text{WO}_4$  (1.76 Å, 926  $\text{cm}^{-1}$ ),  $\text{Na}_2\text{WO}_4$  (1.76 Å, 940  $\text{cm}^{-1}$ ), and  $\text{Al}_2(\text{WO}_4)_3$  (1.76 Å, 1030–1060  $\text{cm}^{-1}$ ).<sup>43</sup> Therefore, the average angular distortion of the  $\text{WO}_4$  tetrahedron in  $\text{Mg}_{2.5}\text{VWO}_8$  structure is estimated to be similar to that in  $\text{Na}_2\text{WO}_4$ .

(36) Schulze, H.; Mueller, A. *Advances in Raman Spectrosc.* **1972**, *1*, 546–549.

(37) Weinstock, N.; Schulze, H. *J. Chem. Phys.* **1973**, *59*, 5063–5067.

(38) Opara Krasovec, U.; Orel, B.; Surca, A.; Bukovec, N.; Reisfeld, R. *Solid State Ionics* **1999**, *118*, 195–214.

(39) Smit, J. P.; Kim, H.-S.; Pless, J. D.; Stair, P. C.; Poepelmeier, K. R. *Inorg. Chem.* **2005**, in press.

(40) Macalik, L. *J. Alloy. Compd.* **2002**, *341*, 226–232.

(41) Guedes, I.; Hirano, Y.; Grimsditch, M.; Wakabayashi, N.; Loong, C. K.; Boatner, L. A. *J. Appl. Phys.* **2001**, *90*, 1843–1846.

(42) Hardcastle, F. D.; Wachs, I. E. *J. Raman Spectrosc.* **1990**, *21*, 683–691.

(43) Hardcastle, F. D.; Wachs, I. E. *J. Raman Spectrosc.* **1995**, *26*, 397–405.

**Table 4.** Assignments and Raman Shifts in cm<sup>-1</sup> of VO<sub>4</sub><sup>3-</sup>, MoO<sub>4</sub><sup>2-</sup>, and WO<sub>4</sub><sup>2-</sup> Tetrahedra in Mg<sub>2.5</sub>VMoO<sub>8</sub> and Mg<sub>2.5</sub>VWO<sub>8</sub><sup>d</sup>

Point group, symmetry species, vibrational mode (all modes are Raman active), and the correlation				Mg <sub>2.5</sub> VMoO <sub>8</sub>		Mg <sub>2.5</sub> VWO <sub>8</sub>	
T <sub>d</sub> : 4 normal modes			C <sub>s</sub> : 9 normal modes		MoO <sub>4</sub> <sup>2-</sup>	VO <sub>4</sub> <sup>3-</sup>	WO <sub>4</sub> <sup>2-</sup>
ν <sub>s</sub> (M-O)	ν <sub>1</sub> , A <sub>1</sub>	→	ν <sub>s</sub> (M-O)	A'	910	860	953
			ν <sub>s</sub> (M-O) <sub>s</sub> <sup>a</sup>		1016 (Mo=O), 974 (Mo <sup>≡</sup> O---Mg)	944 (V <sup>≡</sup> O)	1035 (W=O)
ν <sub>as</sub> (M-O)	ν <sub>3</sub> , T <sub>2</sub>	→	ν <sub>s</sub> (M-O) <sub>s</sub> <sup>a</sup>	A'	807 <sup>b</sup>	799 <sup>b</sup>	892 <sup>c</sup>
			MO <sub>2</sub> scissor		~330-370	387	391
Bending (O-M-O)	ν <sub>2</sub> , E	→	MO <sub>2</sub> wag	A''			
			Deformation				
			MO <sub>2</sub> rock				
			MO <sub>2</sub> twist				
	ν <sub>4</sub> , T <sub>2</sub>	→	ν <sub>as</sub> (M-O)		See ref. 39	~795	See ref. 39

<sup>a</sup> O<sub>s</sub> and O<sub>l</sub> is the oxygen with a shorter and a longer M–O bond length, respectively, than any others. M = V, Mo, W. <sup>b</sup> Estimated for the V/Mo–O bond length of 1.77 Å. <sup>c</sup> Estimated for the W–O bond length of 1.80 Å. The band at 910 cm<sup>-1</sup> seen in Figure 3b, close to 892 cm<sup>-1</sup>, may be attributed to this W–O<sub>l</sub> stretching vibration. <sup>d</sup> See ref 46 for the modes of the C<sub>s</sub> group.

Structural distortion of the tetrahedral MO<sub>4</sub> ion in crystalline solids lowers the tetrahedral T<sub>d</sub> symmetry and the lowered symmetry should be described for more accurate vibrational assignments. A free MO<sub>4</sub> ion of T<sub>d</sub> symmetry has nine normal modes of vibration constituting four frequencies of three different symmetry species, i.e., ν<sub>1</sub>(A<sub>1</sub>), ν<sub>2</sub>(E), ν<sub>3</sub>(T<sub>2</sub>), ν<sub>4</sub>(T<sub>2</sub>). The vibrational representation for the T<sub>d</sub> symmetry is given as follows. Γ<sub>vib</sub>(T<sub>d</sub>) = A<sub>1</sub> + E + 2T<sub>2</sub>. When a single M–O bond length of a tetrahedral MO<sub>4</sub> is shorter (or longer) than any others as in the case of the terminal mono-oxo surface species or MOX<sub>3</sub> (X = F, Cl, Br),<sup>44</sup> the symmetry is lowered from T<sub>d</sub> to C<sub>3v</sub> and the vibrational representation for the C<sub>3v</sub> symmetry, Γ<sub>vib</sub>(C<sub>3v</sub>) is given to 3A<sub>1</sub> + 3E as described in the point group correlation table.<sup>16</sup> Moreover, when another M–O bond length is longer than any other two M–O bond lengths, as in the case of our samples, the symmetry is further lowered to C<sub>s</sub> and the vibrational representation for the C<sub>s</sub> symmetry, Γ<sub>vib</sub>(C<sub>s</sub>) is given to 6A' + 3A'' where all nine vibrations are infrared- and Raman-active. The correlation diagram between T<sub>d</sub> and C<sub>s</sub> is described in the Table 2 only for the symmetric and asymmetric stretching modes for simplicity. Table 2 shows three symmetric stretching frequencies with A' symmetry which correspond to the three (short, medium, and long) bond lengths, in good agreement with the concept of diatomic approximation.<sup>45</sup>

The band appearing at 1016 cm<sup>-1</sup> in Figure 3a and the band appearing at 1035 cm<sup>-1</sup> in Figure 3b should be

attributed to the VO<sub>4</sub> or MoO<sub>4</sub> and VO<sub>4</sub> or WO<sub>4</sub>, respectively. Since vanadium is common to both structures and these two band positions are significantly different, then the possibility of VO<sub>4</sub> related vibrations should be excluded. Accordingly, these bands are attributed to the MoO<sub>4</sub><sup>2-</sup> and WO<sub>4</sub><sup>2-</sup> ions, respectively; the bands at 1016 and 1035 cm<sup>-1</sup> are assigned to the Mo=O and W=O vibrations with the shortest MoO and WO bond length, respectively. The shortest MoO and WO bonds are those which share an oxygen (O(2) and O(7)) with Mg(2) because Mg cation vacancies are localized on the face-shared Mg(2) octahedral sites, as described above. Specifically, one-fourth of the Mg(2) sites are vacant. These vacancies change the coordination environment of O(2) and O(7). Instead of being bonded to two Mg(2) and one V/Mo/W(2) or V/Mo/W(1) (three total bonds), O(2) and O(7) are bonded to only one Mg(2) and one V/Mo/W(2) or V/Mo/W(1) (two total bonds), respectively. The two coordinated oxygen atoms will be more strongly bonded to the higher-valent transition metal ion. This is reflected in the average bond distances obtained from the single-crystal X-ray data (see Table 3 and ref 9) and supports the vibrational assignment of these bands as M=O. For comparison, dehydrated surface Mo=O and W=O stretching vibrations have been observed at 1012 and 1027 cm<sup>-1</sup>, respectively.<sup>20</sup> Although these band positions are similar, the spectra in the present case are not surface-related.

The W=O band at 1035 cm<sup>-1</sup> is broader than the Mo=O band at 1016 cm<sup>-1</sup>, consistent with the wider range of the shortest W=O bond length (see Table 3) of 1.703–1.73 Å

(44) Oyama, S. T.; Went, G. T.; Lewis, K. B.; Bell, A. T.; Somorjai, G. A. *J. Phys. Chem.* **1989**, *93*, 6786–6790.

(45) Hardcastle, F. D.; Wachs, I. E. *J. Phys. Chem.* **1991**, *95*, 5031.

(46) El-Sabban, M. Z.; Danti, A.; Zwolinski, B. J. *J. Chem. Phys.* **1966**, *44*, 1770–1779.

compared to the corresponding Mo=O bond length of 1.713–1.716 Å.<sup>9</sup> The assignments are further supported by the separate Raman measurements for the solid solution between  $\text{Li}_2\text{Mg}_2(\text{MoO}_4)_3$  and  $\text{Mg}_{2.5}\text{VMoO}_8$ , wherein lower concentrations of cation vacancies correlates with a systematic decrease in the oxygen  $p\pi$ –molybdenum  $d\pi$  bonding.<sup>39</sup>

Because one-fourth of the Mg(2) sites are on average vacant, there are two shorter M–O bond lengths in individual  $\text{MO}_4$  groups with  $C_S$  symmetry. One is associated with the vacancies, that is, when O(2) and O(7) are two coordinate as previously described, and the other bond length is associated with the filled Mg(2) sites and O(2) and O(7) are three coordinate. This average structure results in two different  $\nu_s(\text{M}-\text{O}_s)$  frequencies (see Table 4). The  $\text{Mg}^{2+}$  coordination to the oxygen increases the M=O bond length and decreases the M=O bond order and accordingly lowers the M=O stretching frequency. The band at  $974\text{ cm}^{-1}$  shown in Figure 3a is probably due to the stretching vibration of Mo=O type (i.e.,  $\text{Mo}=\ddot{\text{O}}$ ) bonds where the oxygen (O(2) and O(7)) is not associated with Mg(2) vacancies. The possibility that the band at  $974\text{ cm}^{-1}$  may be attributed to V=O or Mo=O double bonds associated with the vacancies was excluded because the Raman band at  $974\text{ cm}^{-1}$  clearly appears in the Raman spectrum for isostructural  $\text{Li}_2\text{Mg}_2(\text{MoO}_4)_3$ , which does not contain cation vacancies or vanadium.<sup>39</sup> All observed Raman frequencies and their assignments, as we understand them at the present time, are summarized in Table 4.

## Conclusions

The crystal structure of  $\text{Mg}_{2.52}\text{V}_{1.09}\text{W}_{0.91}\text{O}_8$  was solved by single-crystal X-ray diffraction and is isostructural with

$\text{Mg}_{2.54}\text{V}_{1.08}\text{Mo}_{0.92}\text{O}_8$  and  $\text{Mn}_{2.47}\text{V}_{0.94}\text{Mo}_{1.06}\text{O}_8$ .<sup>9,11</sup> Raman spectroscopy and X-ray single crystallographic structural data were used to show that the high-frequency Mo=O and W=O stretching vibrations associated with the distorted  $\text{MoO}_4$  and  $\text{WO}_4$  tetrahedra with reduced  $C_S$  symmetry, which appeared at 1016 and  $1035\text{ cm}^{-1}$ , respectively, were associated with the  $\text{Mg}^{2+}$  cation vacancies. These vibrations are similar in energy to the Mo=O and W=O stretching vibrations on dehydrated oxide surfaces.

**Acknowledgment.** The authors gratefully acknowledge the National Science Foundation, Solid State Chemistry (Award Nos. DMR-9727516 and DMR-0312136), the EMSI program of the National Science Foundation at the Northwestern University Institute for Environmental Catalysis (Grant No. 9810378) and the Department of Energy, BES-Chemical Sciences, Geosciences and Biosciences under Grant No. DE-FG0203ER15457 for support of this work. The authors made use of the Central Facilities supported by the MRSEC program of the National Science Foundation (Grant DMR-0076097) at the Materials Research Center of Northwestern University.

**Supporting Information Available:** X-ray crystallographic file in CIF format and differential thermal analysis plot. This material is available free of charge via the Internet at <http://pubs.acs.org>.

IC051740H